J. Phys. B: At. Mol. Opt. Phys. **29** (1996) 2453–2472. Printed in the UK

Observations and theoretical analysis of highly excited singlet and triplet states of cadmium

E Vidolova-Angelova†, C Baharis‡, G Roupakas‡ and M Kompitsas‡§

† Institute of Solid State Physics, Bulgarian Academy of Sciences, 72 Tzarigradsko Chaussee blv, 1784 Sofia, Bulgaria

‡ National Hellenic Research Foundation, Theoretical and Physical Chemistry Institute, 48 Vasileos Konstantinou Ave., 116 35 Athens, Greece

Received 20 November 1995, in final form 15 March 1996

Abstract. We have recorded the $5sn\,^3P^o_J$ ($n = 7$–50) bound Rydberg spectrum of cadmium. We have fully resolved the multiplet up to $n = 19$ and partially up to $n = 24$. Furthermore, we have observed the odd singlet and triplet $5snf$ Rydberg series for $n = 10$–22 and $n = 4$–21, respectively. We have applied two- and three-step laser schemes to excite Cd vapour in a heat pipe-like oven which was operated as a thermionic diode for detection. Theoretical calculations were performed for the energies of the $5snp$ and $5snf$ series using perturbation theory with a zero-order model approximation. There is a good agreement between theoretical and experimental results for the $5snp$ series, the deviation decreasing with n and being 1–2 cm^{-1} for $n = 50$. The agreement for the $5snf$ is satisfactory. From the quantum defect of the $5snf$ series we approximate a value of the effective dipole polarizability of the Cd^+ ion of 19 a_0^3 in units of the Bohr radius.

1. Introduction

In this paper we report our results of two- and three-step resonance ionization studies of the bound Rydberg spectrum of cadmium. This atom is a two-electron system, having in its ground state a $5s^2$ configuration outside a closed shell. Such atoms are very appropriate when one wants to study how the interelectronic interaction in the valence shell manifests itself in the spectrum. Cadmium is homologous to the earth alkaline atom Sr, but in contrast with Sr, the Cd 4d subshell is filled up with 10 electrons and this fact makes both the bound and autoionizing spectra of the two atoms differ essentially. Thus in Sr a 5s electron can easily be excited to the empty 4d subshell and a number of excited states such as $4d5p\,^1P^o_1$ and $4d5s\,^1D_2$ lie below the first threshold and perturb the principal series. This cannot be the case for the Cd atom. Furthermore, some double excitations of the Sr valence electrons (such as the $5p^2$ state) appear as perturbers below the first threshold while the corresponding levels for Cd lie all above its ionization limit.

In the past, there has been more work done, both experimental and theoretical, on the autoionizing part than on the bound spectrum of Cd. Such investigations involved either photoabsorption measurements using a flash tube (Marr and Austin 1969) or a synchrotron (Mansfield 1978, Jimenez-Mier *et al* 1989, Baig *et al* 1994) as a background continuum and revealed 'optically allowed' levels corresponding to odd $J = 1$ one-electron transitions

§ Author to whom all correspondence should be addressed.

0953-4075/96/122453+20$19.50

to $4d^9 5s^2 n\ell$ and to $4d^{10} 5p n\ell$ doubly excited states. Ejected-electron spectra following electron-impact excitation gave information on 'optically forbidden' states (Pejcev *et al* 1977, Hashizume and Wasada 1980, Martin and Ross 1984) of even parity and $J = 1$. On the other side, the data on the bound spectrum are rather scarce. The only systematic study of the Rydberg spectrum resulted from the Cd vapour absorption of background continua, provided by microwave-excited rare-gas lamps (Brown *et al* 1975). These measurements revealed the one-photon excited $5snp\,{}^1P_1^o$ principal series, observed up to $n = 66$, and the Cd ionization limit at 72 540.07 cm^{-1} was obtained from these data. In the same study, the observation of the intercombination transitions to the $5snp\,{}^3P_1^o$ levels, up to $n = 31$, indicated a departure from pure LS coupling of the states. Furthermore, weak lines were observed under relative high vapour pressure and attributed to one-photon quadrupole transitions to the $5snd\,{}^1D_2$ states.

Lifetime measurements of relative low energy levels ($n < 13$) have been deduced by various authors using different experimental techniques. The earliest measurements involved the excitation of Cd vapour by a discharge and the application of the Hanle effect revealed the lifetimes of the even $5s7s\,{}^3S_1$ and $5snd\,{}^3D_J$ ($n = 5$–7) states (Laniepce 1970, Chantepie *et al* 1975, Laniepce *et al* 1976). Combining a discharge with a dye laser, a stepwise excitation allowed the extention of the lifetime measurements to higher triplet ns and nd levels: up to $n = 8$ in an atomic beam experiment (Kerkhoff *et al* 1980) and up to $n = 12$ in a cell experiment (Chantepie *et al* 1983). In particular, the latest results showed the hydrogenic behaviour of the lifetimes of the $ns\,{}^3S_1$ and $nd\,{}^3D_J$ states. This indicates that they are not perturbed, in contrast to what had been observed for the corresponding singlet series which are strongly perturbed by the autoionizing $5p^2\,{}^1S_0$ and ${}^1D_2$ states. This might explain also the fact that the principal $5snd\,{}^1D_2$ series lies lower in energy than the ${}^3D_2$ one (Moore 1955), which is opposite to what is generally expected. Measurements of the energy levels on the $5snf\,{}^{1,3}F_J^o$ series, performed in the present experiment, show a similar behaviour.

In the past, the lack of systematic spectroscopic studies on Cd Rydberg series which do not couple to the ground state by a dipole transition, might be due to the high ionization threshold of this atom and also to the fact that its resonance transitions lie in the UV. The advent of the pulsed dye laser, in combination with multistep excitation schemes, makes it possible that such studies can be extended to other Rydberg series. In the present work, to induce the resonance transitions, a powerful dye laser was used, whose output was either frequency doubled (for the triplet transition) or was used in a non-resonant excitation scheme to populate a singlet level, lying higher in energy, which then decayed radiatively to the desired singlet resonance level. To compensate for the reduced excitation probability of the higher Rydberg states, a heat pipe-like oven with thermionic detection was used, where the final state was transferred into the continuum either by a collision or by absorption of an additional photon. This process becomes more effective when approaching the continuum. Thus, in this work, we have resolved the fine structure of the $5snp\,{}^3P_J^o$ series up to $n = 19$ and extended the observed data to $n = 50$. A theoretical calculation, based on perturbation theory, could reproduce the energies of the observed levels within a few wavenumbers. Furthermore, we have measured the level energies of the $5snf\,{}^{1,3}F_J^o$ series and in a short discussion we give an estimate of the dipole polarizability of the Cd^+ ion.

The spectroscopy of the heavy metal Cd has recently gained particular interest due to the increased problems in pollution. Therefore, laser-based spectroscopic techniques of high sensitivity are needed which will allow the determination of this highly toxic element in order to control its levels in biological and environmental substances. The resonance ionization spectroscopy (RIS), close related to the one applied in this experiment, and an

accurate knowledge of the atomic spectrum will give rise to appropriate excitation schemes which may further reduce the limits of detection.

2. Experimental technique

The experimental set-up has been presented in detail previously (Kompitsas *et al* 1994), so only a brief description will be given here (figure 1). A 10 Hz pulse generator drove the two laser systems, and their pulse delay and sequence could be synchronized within nanoseconds with homemade electronics. One laser system was a Nd:YAG pumped dye laser (Quantel Datachrom), tunable in the visible and near ultraviolet region. The second one was a (Lumonics) excimer laser pumping a commercial (EPD 330) and a homemade dye laser, both consisting of a Littman-type oscillator and an amplifier. When recording the spectra, a portion of the third tuned laser was sent into a Ne optogalvanic lamp and to a Fabry–Perot interferometer (free spectral range 1 cm^{-1}), which provided the absolute and the relative wavelength calibration, respectively. This method allowed an absolute accuracy of 0.2 cm^{-1} for the final laser transition.

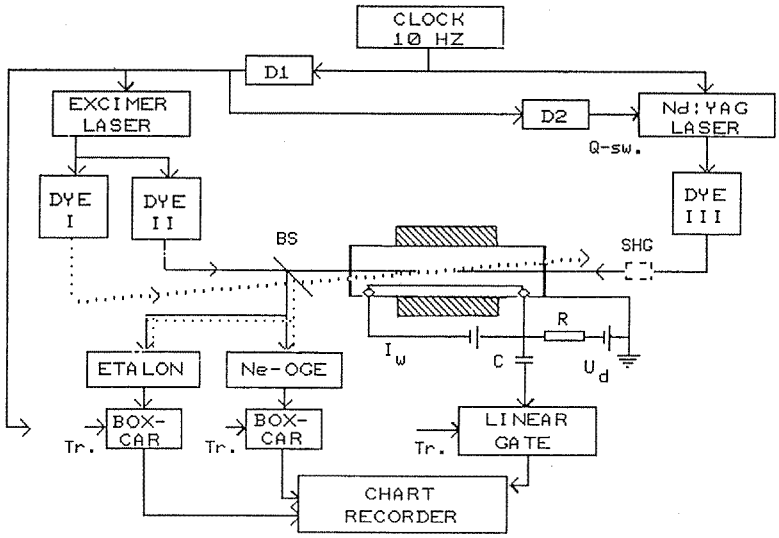

Figure 1. Experimental set-up: D1, D2 delays; Q-sw, Q switching of the Nd:YAG laser; BS, beam splitter; Tr, trigger pulses; SHG, second harmonic generating crystal; U_d, diode voltage; I_w, wire heating current; R, resistor; C, coupling capacitor; OGE, neon optogalvanic spectrum.

The Cd vapour was confined in a cylindrical stainless steel heat pipe-like oven, 42 cm long. The heated zone (15 cm long in the middle) was kept at 320–350 °C. At both ends of the tube, the vacuum pipes and the buffer gas line were connected. A few millibars of Argon buffer gas were used to reduce vapour diffusion and protect the windows. We measured no systematic energy level shifts for this buffer gas pressure. A single stainless steel wire (0.3 mm in diameter) along the tube was used as the thermionic detector, working in the space-charge-limited regime (Popescu *et al* 1966). The wire was directly heated by a current of 1.5 A to enhance the signal. A second circuit biased the wire to 1.5 V through a 100 kΩ resistor while the tube was grounded. A 20 pF capacitor coupled the signal to a linear gate (ORTEC Mo. 9415) and its output was sent to the chart recorder.

3. Excitation schemes

In this experiment, we started from the ground state and measured the odd triplet and some singlet 5s*n*p states. We also recorded a part of the odd triplet and singlet 5s*n*f spectrum and under special conditions we observed a number of lines that we could assign to some even triplet 5s*n*s and 5s*n*d energy levels. In figure 2 we present the various excitations schemes that we used to record the spectra together with the relevant part of the Cd spectrum.

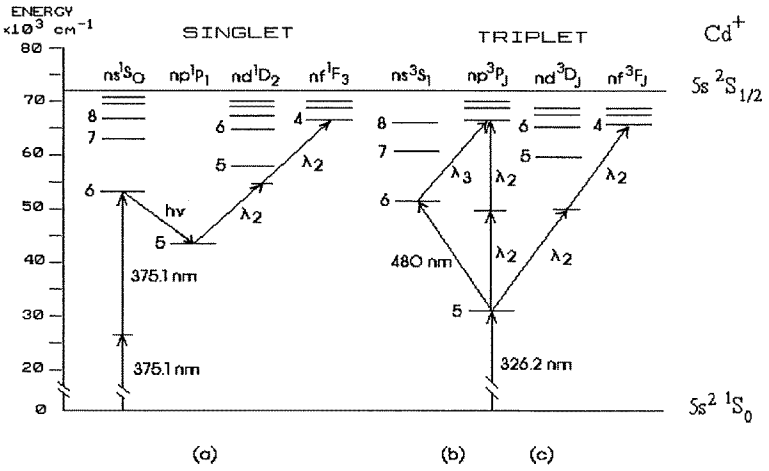

Figure 2. Part of the Cd energy level diagram with the various laser excitation schemes used in this experiment.

3.1. Triplet 5*snp spectra*

To record these spectra, we used the three-step excitation scheme (b) shown in figure 2. In the first step, the 5s5p $^3P_1^o$ was selected using the Datachrom laser output, doubled in a KDP crystal to deliver 326.2 nm. The homemade dye laser was then sent counterpropagating to the first beam and set at 480 nm to resonantly populate the 5s6s $^3S_1$ state. Both lasers were linearly polarized horizontally. For the third step, the Lumonics dye laser beam crossed the first two lasers in the centre of the Cd oven under a small angle and its wavelength λ_3 was tuned in the 562–475 nm region, using the dyes Coumarin 153, 307 and 102, to induce the 5s*n*p transitions. The third laser was linearly polarized vertically. The delays of the three laser beams were set appropriately to maximize the signal.

3.2. Singlet and triplet 5*snf spectra*

Recently (Kompitsas *et al* 1994), we have deduced the dipole polarizability α of the Zn^+ ion from level energy measurements of the Zn 4s*n*f $^{1,3}F_J^o$ Rydberg series. The theoretical model we applied (Van Vleck and Whitelaw 1933) was based on the approximation that the singlet–triplet splitting was small and could be neglected in the calculation. Indeed from Brown *et al* (1975), as well as from our data on the Zn 4s*n*f series, we showed that this condition is fulfilled for Zn. Since for Cd we have no information on this splitting and in order to be able to apply the above model successfully, we measured the singlet and triplet 5s*n*f series separately.

For the $5sn\mathrm{f}\,^1\mathrm{F}_3^o$ series we employed the excitation scheme (a) (see figure 2) with the $5s5p\,^1\mathrm{P}_1^o$ as intermediate level. Since the wavelength of 229 nm for the transition $5s^2\,^1\mathrm{S}_0 \rightarrow 5s5p\,^1\mathrm{P}_1^o$ was not available, we populated this level by a two photon, non-resonant step to the $5s6s\,^1\mathrm{S}_0$ state which decayed radiatively to the $^1\mathrm{P}_1^o$ intermediate state. For this transition the excimer-pumped dye laser was focused in the centre of the Cd oven with a wavelength fixed at 375.1 nm (QUI, Lambda Physik). To check the population efficiency of this scheme, we recorded transitions to the $5sns\,^1S_0$ and the $5snd\,^1\mathrm{D}_2$ levels for $n < 15$ with a second laser and their energies agreed well with known data (Moore 1955, Brown *et al* 1975) within our experimental accuracy. To record the $5sn\mathrm{f}\,^1\mathrm{F}_3^o$ series, we induced a two-photon, non-resonant transition by tuning the Datachrom laser in the 720–690 nm range (LD 700, Exciton). We focused the beam in the centre of the oven such as to coincide with the first beam maximizing the signal.

For the $5sn\mathrm{f}\,^3\mathrm{F}_J$ series, we applied the excitation scheme (c) in figure 2. The $5s5p\,^3\mathrm{P}_1^o$ state was populated in the same way as in section 3.1 to record the triplet $5sn\mathrm{p}$ series. The second laser induced a two-photon, non-resonant transition and its wavelength λ_2 was tuned using the dyes Coumarin 153, 307 and 102. The laser beam was slightly focused in the oven centre. We observed only one peak, so no fine structure of this triplet series could be resolved.

4. Calculation method

The energies of the Cd $5sn\mathrm{p}$ and $5sn\mathrm{f}$ states have been calculated by using a perturbation theory (PT) with a zero-order model approximation. The method is formally exact and the only experimental information needed is the ionization energy of the valence electron. This method has been successfully applied for investigating highly excited states of rare earths (Vidolova-Angelova 1992, Vidolova-Angelova and Ivanov 1991) and recently of the alkaline earth element Sr (Vidolova-Angelova 1994). One can find a detailed description of our calculation method in the cited papers. Here we consider only the details connected with the present calculation.

4.1. Model potential

The ground electron configuration of the Cd atom is $4\mathrm{d}^{10}5\mathrm{s}^2$, the nuclear charge $Z = 48$ and the ionization energy 72 540.07 cm^{-1} (Brown *et al* 1975). In the zero-order approximation of our method, both valence electrons are considered as independent and moving in the core ($4\mathrm{d}^{10}$) field. A model potential V_{mod} describes their movement. Solving the Dirac equations with V_{mod} one obtains a set of one-electron wavefunctions and one-electron energies ε_0 that are the basis of the PT. Now we study the states $5sn\ell$, i.e. one valence electron is in its ground state and the other one is excited to a Rydberg state. As usually, V_{mod} depends only on one fitting parameter Φ determined by the ionization energy of the electron,

$$\begin{aligned} V_{\mathrm{mod}}(r/\beta) = {} & (2/rZ)[1-\exp(-2r)(1+r)] + (8/rZ) \\ & \times[1-\exp(0.8r)(1+0.6r+0.16r^2+0.032r^3)] \\ & +((N-10)/rZ)[1-(1+\beta r+\beta^2 r^2+\gamma r^3)^{-1}], \end{aligned} \tag{1}$$

with $\gamma = 0.01(N-10)/Z^3$, where $N = 46$ is the number of the core electrons. V_{mod} in (1) is used for the 5s electron: its ionization energy is 136 374.74 cm^{-1} (see the energies of Cd^+ Moore (1955)). The same value is obtained as an eigenvalue when solving the Dirac equations if $\beta = 0.057\,68$.

Our experience shows that fast convergence of the PT series is guaranteed when in the zero-order approximation one considers most of the effects. This is the reason to regard the excited $n\ell$ electron in another model potential, taking into account the screening of the core field by the 5s electron. This effect was proved to be very strong for Sr (Vidolova-Angelova 1994) and for Cd. Indeed, the 5s electron is rather more closely located to the core than the np electron: the average radius of the 7p electron is about six times larger than that of the 5s electron. For the $n\ell$ electron an additional term to $V_{\rm mod}$ accounts for the screening:

$$V_{\rm scr} = (1/rZ)[1 - (1 + \beta r + \beta^2 r^2 + \gamma r^3)^{-1}]. \tag{2}$$

A similar procedure was employed for Sr (Vidolova-Angelova 1994). The parameter β for np was varied while obtaining a minimum energy at $\beta = 0.048$. $V_{\rm scr}$ in (2) accounts almost entirely for the monopole direct interaction between the electrons. Indeed, the correction to zero order of the one-electron energy

$$\delta\varepsilon_0 = -\langle n\ell j|V_{\rm scr}|n\ell j\rangle \tag{3}$$

caused by (2) practically ignores the corresponding radial integral R_0.

In the zero-order approximation, the independent valence electrons are regarded in the jj-coupling scheme. Transition to the true intermediate coupling scheme is performed after the construction of the energy matrix and its diagonalization.

4.2. First-order PT

The interaction between the valence electrons is considered in the first-order PT, where the Coulomb interaction between them is calculated exactly. The correction to the energy ΔE_1 from this interaction is expressed through the corresponding angular parts and radial integrals R_λ. Therefore, the energy of the two-electron system is

$$E(5sn\ell) = \varepsilon_0(5s) + \varepsilon_0(\widetilde{n\ell}) + \delta\varepsilon_0(\widetilde{n\ell}) + \Delta E_1. \tag{4}$$

The mark ˜ denotes that the $n\ell$ electron is considered in the $V_{\rm mod} + V_{\rm scr}$ potential.

It is assumed that $V_{\rm mod}$ and $V_{\rm scr}$ take effectively into account the interaction of different series including the interaction with the continuum. For example, the potential $V_{\rm scr}$ effectively considers the interaction with all states of the excited valence core. The successful application of the method and the good accuracy confirm this conclusion. For this reason, we include in the energy matrix only the states of the investigated 5snp or 5snf configuration and its order is two (for 5snp ($J = 1$) and 5snf ($J = 3$)) or one (for all other investigated series).

The described procedure was applied for calculating the investigated states 5snp, $n = 7$–15 as well as for the 5snf states with $n = 4$–9. It should be noted that the used theoretical method is asymptotically exact, because the non-considered effects decrease as $1/n^3$. This means that the calculated values are more accurate for higher n (see table 1), but unfortunately it is not possible to calculate the wavefunctions for high enough n, because the error from the calculation procedure itself (not from the method) accumulates, and for a determined value n ($n > 17$ for 5snp and $n > 9$ for 5snf) this error is so big that the wavefunctions become diverging.

4.3. Extrapolation

The energies for higher n ($n > 15$ in the case of 5snp states) are obtained by an extrapolation procedure. The zero-order one-electron energies and the radial integrals are separately

Table 1(*a*). Theoretical and experimental energies of the 5s*n*p $^3P_0^o$ states: +, values taken from Moore (1955).

n	$E_{theor.}$	$E_{exp.}$
7	65 027.9	64 995.9$^+$
8	67 847.7	67 829.6$^+$
9	69 325.4	69 314.0
10	70 198.9	70 191.4
11	70 758.6	70 753.4
12	71 138.9	71 135.4
13	71 409.2	71 406.4
14	71 608.2	71 606.1
15	71 759.4	71 757.4
16	71 876.7	71 874.6
17	71 969.6	71 967.4
18	72 044.3	72 041.8
19	72 105.4	72 102.9

extrapolated using the mean square method. The extrapolation expression is

$$R_y(-1/n^2 + \alpha/n^3 + b/n^4 + \cdots) \tag{5}$$

where $R_y = 109\,736.78$ cm^{-1} (Brown *et al* 1975). The first term in (5) is eliminated when extrapolating the radial integrals and $\delta\varepsilon_0$. The maximum divergence from the exactly calculated values was 2.6 cm^{-1}.

We can estimate the quality of the extrapolation and its error by comparing the exactly calculated energies ($n = 7$–15 for 5s*n*p) with their values obtained by the extrapolation. In such a way we evaluate an extrapolation error of about 0.1–0.2 cm^{-1}. The same error proved to be one order of magnitude higher for the 5s*n*f states, which is connected with the lower number of exactly calculated values (only $n = 4$–9). This caused the extrapolation of the 5s*n*f energies to be realized in another way. In this case, the energies of the two-electron 5s*n*f states themselves were extrapolated using the expression

$$E(n) = I_i + R_y(-1/n^2 + \alpha/n^3 + \cdots). \tag{6}$$

In this way, the extrapolation error for the 5s*n*f states became $\sim$ 0.5–0.8 cm^{-1} so that the extrapolation might be considered as reliable.

5. Results and discussion

5.1. 5s*n*p *spectra*

The obtained results (experimental and theoretical) are presented in tables 1(*a*)–(*c*) for the levels with total angular momentum $J = 0$–2, respectively. A gradual increase of the calculation accuracy with n is clearly shown, because the effects, which were not accounted for, decrease as $1/n^3$. The deviation from the experimental data decreases with n and reaches a value of 1–2 cm^{-1} at $n = 50$, being minimum for the $J = 2$ series and maximum for the singlet series. Having in mind that in the calculation the interaction with the excited core states is not considered, we can conclude that the influence of such states is dominant namely for the singlet series. Possible perturbers are available in Moore (1955).

The 5s*n*p terms are normal in the investigated region: $^3P_0 < {}^3P_1 < {}^3P_2 < {}^1P_1$. According to the calculation, at $n = 19$ the energy distribution of the $^3P_0^o$ and $^3P_1^o$ terms is

Table 1(*b*). Theoretical and experimental energies of the $5sn\mathrm{p}\,^{1,3}\mathrm{P}_1^{\mathrm{o}}$ states.

	$5sn\mathrm{p}\,^3\mathrm{P}_1$			$5sn\mathrm{p}\,^1\mathrm{P}_1$		
n	$E_{\mathrm{theor.}}$	$E_{\mathrm{exp.}}$	Moore (1955)	$E_{\mathrm{theor.}}$	$E_{\mathrm{exp.}}$	Moore (1955)
7	65 049.6	65 025.5	65 026.71	65 625.8		65 501.41
8	67 858.4	67 842.0	67 842.06	68 119.9		68 059.39
9	69 331.5	69 320.9	69 320.89	69 473.6		69 439.13
10	70 202.7	70 195.7	70 195.7	70 288.8		70 267.37
11	70 761.2	70 756.4	70 756.39	70 817.4	70 803.1	70 803.25
12	71 140.7	71 137.3	71 137.42	71 179.5	71 170.3	71 169.73
13	71 410.5	71 407.8	71 408.07	71 438.4	71 431.3	71 431.35
14	71 609.2	71 607.2	71 606.98	71 629.9	71 624.9	71 624.61
15	71 760.2	71 758.2	71 758.22	71 776.1	71 771.6	71 771.43
16	71 877.3	71 875.2	71 875.22	71 890.1	71 886.1	71 885.53
17	71 970.0	71 967.7	71 967.85	71 980.5		71 975.97
18	72 044.7	72 042.1	72 042.31	72 053.4		72 048.92
19	72 105.7	72 103.1	72 103.22	72 113.1		72 108.62
20	72 156.1	72 153.4	72 153.65	72 162.6		72 157.98
21	72 198.3	72 195.6	72 195.94	72 204.0		72 199.39
22	72 233.9	72 231.2	72 231.63	72 239.0		72 234.41
23	72 264.2	72 261.6	72 262.05	72 268.8		72 264.26
24	72 290.3	72 287.8	72 288.04	72 294.4		72 289.96
25	72 312.9		72 310.7	72 316.6		72 312.21
26	72 332.5		72 330.36	72 335.9		72 331.67
27	72 349.7		72 347.39	72 352.9		72 348.65
28	72 364.8		72 362.61	72 367.8		72 363.71
29	72 378.2		72 376.12	72 381.0		72 377.05
30	72 390.2		72 387.97	72 392.7		72 388.88
31	72 400.8		72 398.76	72 403.2		72 399.52
32	72 410.4			72 412.6		72 409.03
33	72 419.0			72 421.1		72 417.61
34	72 426.7			72 428.7		72 425.42
35	72 433.8			72 435.7		72 432.47
36	72 440.2			72 441.9		72 438.89
37	72 446.0			72 447.7		72 444.76
38	72 451.4			72 452.9		72 450.14
39	72 456.3			72 457.7		72 455.07
40	72 460.8			72 462.2		72 459.62
41	72 464.9			72 466.3		72 463.82
42	72 468.8			72 470.0		72 467.65
43	72 472.3			72 473.5		72 471.24
44	72 475.6			72 476.7		72 474.59
45	72 478.6			72 479.7		72 477.66
46	72 481.5			72 482.5		72 480.5
47	72 484.1			72 485.1		72 483.17
48	72 486.6			72 487.5		72 485.7
49	72 488.9			72 489.8		72 488.05
50	72 491.0			72 491.9		72 490.24

~ 0.3 cm^{-1} and becomes $\sim$ 0.1–0.2 cm^{-1} for higher n. Therefore, these two series can be considered as merging in energy for $n > 20$. The two triplet series with $J = 1$ and 2 also merge at $n > 24$. The deviation of the singlet term is ~ 1 cm^{-1} at $n = 50$. Similar properties are experimentally observed.

The lowest series members (n = 9–11) that we recorded (excitation scheme (b) in

Table 1(*c*). Theoretical and experimental energies of the $5snp\,{}^3P_2^o$ states.

n	$E_{\text{theor.}}$	$E_{\text{exp.}}$	Moore (1955)
7	65 100.9	65 093.3	65 092.8
8	67 884.5	67 875.2	67 875.2
9	69 346.6	69 339.8	69 340.2
10	70 212.2	70 207.5	70 207.3
11	70 767.5	70 764.2	
12	71 145.2	71 142.8	
13	71 413.7	71 411.6	
14	71 611.6	71 610.2	
15	71 762.1	71 760.5	
16	71 878.7	71 876.9	
17	71 971.1	71 969.1	
18	72 045.5	72 043.2	
19	72 106.3	72 104.0	
20	72 156.6	72 154.1	
21	72 198.7	72 196.3	
22	72 234.2	72 231.7	
23	72 264.5	72 262.1	
24	72 290.5	72 288.2	
25	72 313.0	72 310.7	
26	72 332.6	72 330.2	
27	72 349.7	72 347.4	
28	72 364.9	72 362.5	
29	72 378.3	72 376.0	
30	72 390.2	72 388.0	
31	72 400.8	72 398.7	
32	72 410.4	72 408.3	
33	72 418.9	72 416.9	
34	72 426.7	72 424.9	
35	72 433.7	72 432.0	
36	72 440.2	72 438.4	
37	72 446.0	72 444.3	
38	72 451.3	72 449.7	
39	72 456.2	72 454.7	
40	72 460.7	72 459.2	
41	72 464.9	72 463.6	
42	72 468.7	72 467.4	
43	72 472.2	72 471.0	
44	72 475.5	72 474.2	
45	72 478.6	72 477.5	
46	72 481.4	72 480.2	
47	72 484.1	72 483.2	
48	72 486.5	72 485.4	
49	72 488.8	72 487.8	
50	72 491.0	72 490.2	

figure 2) are shown in figure 3. All three fine structure components were resolved to $n = 19$. For higher n, the $^3P_0^o$ and the $^3P_1^o$ lines merge into each other and only two peaks are observed to $n = 24$. At $n > 24$ only one line is observed. Note that the measured energies of the states $^3P_0^o$, $n = 7$–19, and $^3P_2^o$, $n = 7$–50, are presented for the first time (tables 1(*a*)–(*c*)). If we consider that the two first lasers induce π-transitions ($\Delta m_J = 0$) and the third one a σ-transition ($\Delta m_J = \pm 1$), then only the two $^3P_1^o$ and $^3P_2^o$ series should

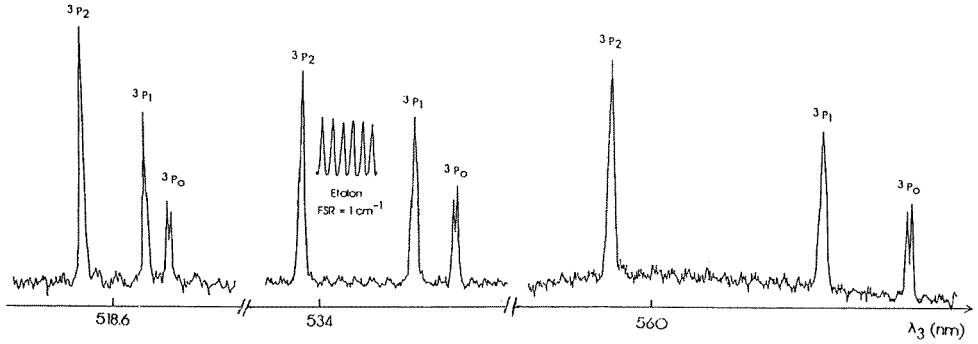

Figure 3. The three-step excitation spectrum 5s*n*p for $n = 9$–11 (from right to left), recorded with the excitation scheme (b). The doublet in the $J = 0$ component is due to the HFS splitting of the 5s6s $^3S_1$ intermediate state.

be excited. Obviously the observation of the $^3P_0^o$ state is due to the mixing of the m_J sublevels, induced by collisions in the two intermediate states.

It is seen from figure 3 that the double peak of the $^3P_0^o$ component remains unchanged although the multiplet splitting is reduced up to one third. This doublet is explained by the hyperfine structure (HFS) of the second intermediate state 5s6s $^3S_1$: 25% of the natural mixture of Cd consists of two odd isotopes and this gives rise to a HFS splitting of 0.6 cm^{-1}. Both HFS components are populated, either by the finite linewidth of the second laser or/and by collisions. The transitions corresponding to the even isotopes merge with the one from the lowest energy of the HFS doublet and cannot be resolved. Due to the same effect, the other two components, $^3P_1^o$ and $^3P_2^o$, indicate that they are also multiple lines. Level positions and line strengths of the four transitions connecting the 5s6s level with each of the 5s*n*p $^3P_1^o$ and $^3P_2^o$ levels are given in Lewis (1977).

Figure 4(*a*) displays the theoretical quantum defects δ for all the 5s*n*p, $n = 7$–15, series according to the formula

$$\delta = n - [R_y/(I - E_n)]^{-1/2}. \tag{7}$$

δ is constant for all series: ~ 3.1 for the triplet series and ~ 3 for the singlet series. For higher n, δ seems slightly to decrease, but in the framework of the calculation inaccuracy δ can be considered as a constant value for every series in the whole investigated region. In figure 4(*b*) the experimental quantum defects are shown up to $n = 50$. For $n > 24$ only one δ value is given, the one for the $J = 2$ level. Within the error bars (calculated on the base of the experimental accuracy of 0.3 cm^{-1}), the quantum defect can be regarded as constant along the series.

In figure 5 we present a part of the same spectrum for n values between 30 and 40. The two spectra are obtained at different intensity I_3 of the third tunable laser. The bottom spectrum, corresponding to lower I_3, consists of narrow lines. The weak peaks on the blue side of the lines with $n < 35$ are the 5s*n*p $^1P_1^o$ energy levels. They can also be excited from the triplet 5s6s intermediate state as a result of the partial breakdown of the LS coupling, already observed in this atom (Brown *et al* 1975). The presence of the singlet states is caused by the mixing of the triplet and singlet states with $J = 1$. One can see in table 2 the wavefunction coefficients for the $J = 1$ states upon diagonalization of the energy matrix. The mixing of the 5s*n*p ($J = 1$) states is significant: the self-contribution of the $^3P_1$ state is $\sim 75\%$ for $n = 7$–15 and reduces to $\sim 66\%$ at $n = 50$. Therefore the mixing of both

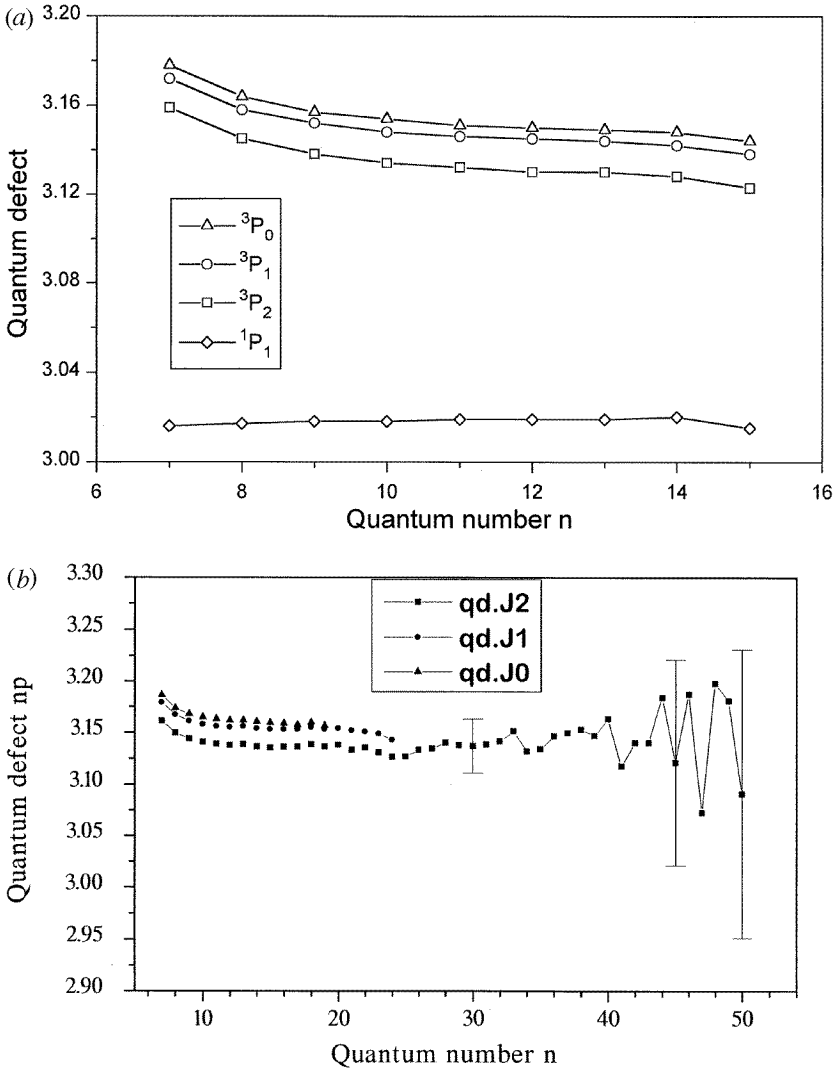

Figure 4. (*a*)Theoretical quantum defects of the 5s*n*p series. (*b*) Experimental quantum defects of the triplet 5s*n*p series.

$J = 1$ states grows with n, which explains the observation also of 5s*n*p $^1P_1^o$ states in both stepwise excitation schemes applied.

The top spectrum in figure 5 is recorded with increased intensity I_3. The broadening of the main lines might be explained as depletion broadening, since the increased intensity leads to an absorption of a further photon with λ_3 which ionizes the atom. The weak peaks between the main profiles have been identified as 5s*n*s $^3S_1$ levels: they have an average quantum defect of 3.57, which agrees well with the calculated value of 3.65 for the same series (Moore 1955). Similarly, for medium n values around 19–22 and for increased I_3, we have observed weak peaks between the 5s*n*p $^3P_J^o$ multiplet and the corresponding $^1P_1^o$ level. We have identified them as 5s*n*d $^3D_3$ with an average quantum defect of 2.08 which coincides well with the one deduced from the $^3D_3$ levels in Moore (1955). The level energies of 5s*n*s and 5s*n*d and their quantum defects are listed in table 3.

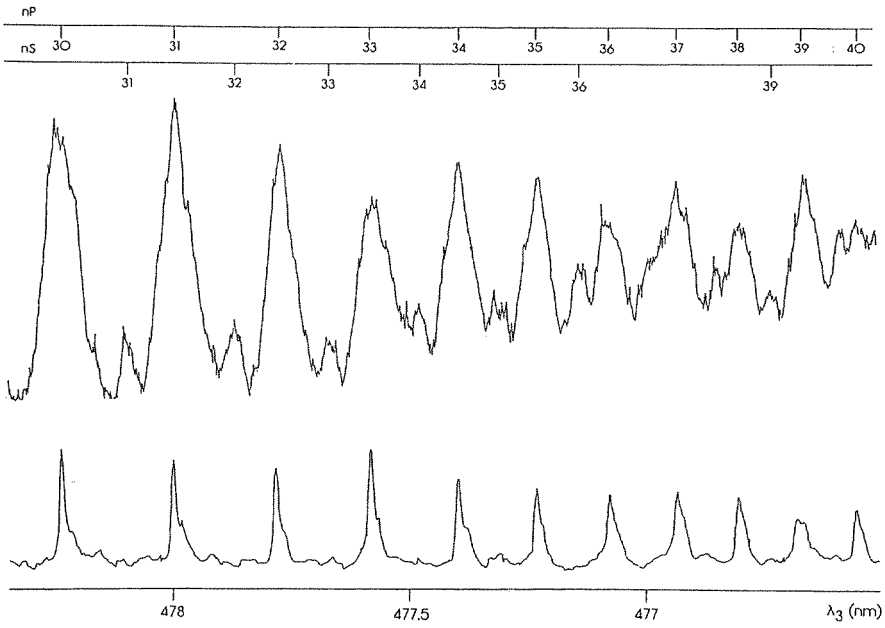

Figure 5. Three-step excitation spectra (scheme (b)) of the 5s*n*p series between $n = 30$ and 40: top; high intensity of the third laser; bottom, low laser intensity.

Table 2. Wavefunction mixing coefficients (in absolute values) of the 'triplet' 5s*n*p states describing the triplet character (left column) and singlet character (right column) (first-order PT with zero-order model potential).

n	$n\mathrm{p}\,^3\mathrm{P}_1$	$n\mathrm{p}\,^1\mathrm{P}_1$
7	0.859 73	0.510 74
8	0.863 69	0.504 02
9	0.865 97	0.500 09
10	0.867 45	0.497 52
11	0.868 53	0.495 64
12	0.869 26	0.494 36
13	0.869 91	0.493 21
14	0.870 24	0.492 63
15	0.870 06	0.492 94
16	0.868 97	0.494 86
17	0.866 34	0.499 46

To explain how these weak peaks emerge through the excitation scheme (b) that we have used, let us consider the one photon transition from the second intermediate 5s6s $^3\mathrm{S}_1$: dipole transitions to the $^3\mathrm{S}_1$ and to the $^3\mathrm{D}_3$ levels are forbidden, corresponding to a change of $\Delta\ell = 0$ and $\Delta\ell = 2$, respectively. Nevertheless, such dipole forbidden transitions have also been observed by other authors who used thermionic detectors and have been explained by ℓ-mixing processes, which are due either to collisions of the excited atom with neutral atomic perturbers in the oven (Burkhardt *et al* 1986, Zhang and Lu 1987, Wu *et al* 1990) or by the local Stark effect (Zhang *et al* 1992) induced by the bias voltage of the thermionic detector. In our experiment, either process could mix some p character

Table 3. Experimental energies of the triplet 5s*n*s and 5s*n*d states populated by a dipole-forbidden transition from the 6s $^3S_1$ state.

5s*n*s ^{3}S			5s*n*d ^{3}D		
n	$E_{exp.}$	n^*	*n*	$E_{exp.}$	n^*
31	72 394.1	27.42	17	72 047.1	14.92
32	72 404.3	28.43	18	72 107.1	15.92
33	72 413.3	29.42	19	72 156.5	16.91
34	72 421.4	30.41	20	72 198.4	17.92
35			21	72 233.6	18.92
36	72 436.0	32.47	22	72 263.6	19.92
37					
38					
39	72 452.6	35.42			

into the wavefunctions of the $^3S_1$ and $^3D_3$ states: this part would then be excited from the 5s6s $^3S_1$ intermediate by the third dipole transition.

Since we were interested primarily in a spectroscopic study of Cd, our experimental conditions differed from those of previous authors by trying to keep those parameters that might affect the spectrum as low as possible. Therefore, we believe that the buffer gas pressure of approximately 1 mbar Ar is too low to induce a collisional ℓ-mixing. Similarly, the laser intensities were of the order of some hundreds of μJ/p or less in order not to broaden the resonances and loose resolution. However, in one respect our experiment differs significantly from previous ones which, we believe, is crucial for the observation of the forbidden lines: all our observed peaks grow out of a continuous ionization signal due to the resonance excitations to the intermediate states induced by the first two laser beams (this was unavoidable, since we identified the intermediate states through their ionization). This resulted in a large number of charges produced along the laser beams, which came as an additional to the bias voltage of the detector, voltage drop along the wire and emitted space charge around it. The effective DC field acting in the active volume can mix some p character into the atomic wavefuctions (from the literature, typical values are some per cent) and let the forbidden lines be excited. A qualitative explanation of the effect of the increased energy of the third laser in figure 5 is as follows. For low energy, the forbidden lines are 'buried' in the continuous ionization signal. As the laser energy is increased, the peaks gain intensity and emerge out of the continuum. It seems that they are also power broadened, as the dipole-allowed *n*p peaks clearly are, so that the ratio of their magnitude cannot reflect the mixing in the wavefunctions.

Under the present experimental conditions, a quantitative treatment of the above effect is not possible. In particular, the contribution of the laser-produced charges to the effective DC field cannot be calculated: besides the spatial variation of the laser intensity over the active volume in the oven, necessary atomic parameters such as absolute excitation and ionization cross sections for Cd are not known. Such a treatment is not the purpose of the present work either. To gain more insight into the mechanisms causing the above transitions, a field- and collision-free environment, such as a Cd atomic beam with a well defined geometry of interaction volume, should be used which is now under preparation.

5.2. 5s*n*f *spectra*

The 5s*n*f $^1F^o_3$ states were observed by scheme (a) and the 5s*n*f $^3F^o_J$ states by scheme (c) in figure 2. Table 4 includes the obtained results. We observed the 5s*n*f $^1F^o_3$ series members

for $n = 10$–22. For $n < 10$, the dye efficiency was too low to induce the two-photon transition while for $n > 22$ the signal was too weak. The $5snf\,{}^3F^o_J$ series was observed also to $n \sim 20$, because the higher series members merged with the $5s(n+3)p\,{}^1P^o_1$ levels (which are also excited by this excitation scheme) and could not be resolved any more.

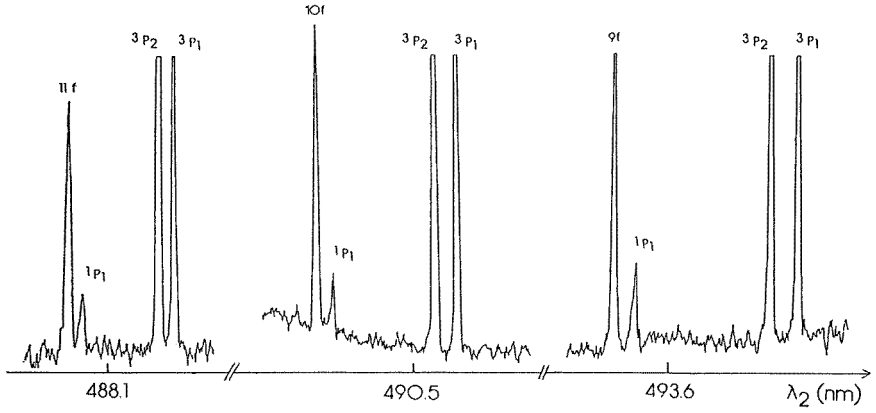

Figure 6. Two-step laser excitation (scheme (c)) in the lower part of the spectrum. From right to left: $5snp\,{}^{1,3}P_J$ for $n = 12$–14, $5snf\,{}^3F_J$ for $n = 9$–11.

A part of the observed ${}^3F^o_J$ spectrum (scheme (c)) is shown in figure 6. According to the selection rules for a two-photon, non-resonant transition from the odd 5s5p state, we expect to populate the odd triplet $5snp$ as well as the $5snf$ states. However, besides the expected transitions, we also recorded the singlet $5snp$ series, due to the cited reasons above. The measured energy levels of the two $5snp\,{}^3P_{1,2}$ components from these spectra are in good agreement ($\Delta E < 0.4$ cm^{-1}) with the corresponding values obtained by the three laser experiment (scheme (b)).

We have not observed the $5snp\,{}^3P^o_0$ series in this $(1+2)$-photon excitation scheme, in contrast to the observations of the previous section 5.1. This can be explained as follows. The first laser is linearly polarized horizontally (π-light, $\Delta m_J = 0$). The second laser beam inducing the two-photon, non-resonant transition is linearly polarized vertically (σ-light). According to the two-photon selection rules (Melikechi and Allen 1986) this implies $\Delta m_J = \pm 2$. Without collisions in the intermediate state, the final state would have $J = 2$ only. Taking the collisional mixing into account as was shown in the previous section, it results additionally to the population of states with $J = 1, 3$ but not $J = 0$.

The simple pattern shown in figure 6 was observed when the second laser was operated with the dyes Coumarin 153 and 307. The gain profile of Coumarin 102 includes the wavelength 480 nm which induces the one-photon transition to the 5s6s ${}^3S_1$ state (see section 5.1). This fact, combined with the focusing of the second laser needed to induce the two-photon ($2\omega_2$) transition, has a dramatic effect on the obtained spectrum for medium n values up to threshold. In figure 7 the familiar pattern corresponding to the $(\omega_1 + 2\omega_2)$ two-colour spectra is shown for $n = 16$–19. Additionally, groups of two strong lines followed by two weak peaks appear systematically between the $2\omega_2$ spectrum. We could not assign these lines to any series when we calibrated their energy as $E(5s5p) + 2\omega_2$. It turned out that they correspond to one-photon transitions from the 5s6s ${}^3S_1$ state, this having been populated by the non-coherent broadband emission part of the focused second laser (amplified spontaneous emission, ASE). In each group, the two strong peaks are assigned

Table 4. Theoretical and experimental energies of the $^{1,3}F^o_J$ states.

	nf ^{3}F$_2$	nf ^{3}F$_3$	nf ^{3}F$_4$	nf ^{3}F$_J$	nf ^{1}F$_3$	
n	$E_{\text{theor.}}$	$E_{\text{theor.}}$	$E_{\text{theor.}}$	$E_{\text{exp.}}$	$E_{\text{theor.}}$	$E_{\text{exp.}}$
4	65 273.0	65 272.5	65 271.9	65 586.0	65 283.7	
5	67 931.9	67 931.7	67 931.4		67 940.4	
6	69 361.9	69 361.7	69 361.5	69 456.4	69 367.7	
7	70 217.1	70 217.2	70 217.5	70 277.4	70 221.5	
8	70 770.7	70 770.8	70 770.9	70 809.7	70 773.8	
9	71 146.7	71 146.9	71 147.2	71 174.2	71 149.2	
10	71 414.8	71 415.0	71 415.3	71 434.1	71 416.7	71 433.3
11	71 612.3	71 612.5	71 612.8	71 627.0	71 613.9	71 626.1
12	71 762.1	71 762.3	71 762.5	71 773.3	71 763.3	71 772.2
13	71 878.3	71 878.5	71 878.7	71 887.2	71 879.3	71 886.4
14	71 970.3	71 970.5	71 970.7	71 977.6	71 971.2	71 976.8
15	72 044.4	72 044.5	72 044.7	72 050.6	72 045.1	72 049.5
16	72 104.9	72 105.0	72 105.2		72 105.5	72 109.1
17	72 155.0	72 155.1	72 155.2		72 155.5	72 158.5
18	72 196.8	72 196.9	72 197.1	72 200.7	72 197.3	72 199.8
19	72 232.3	72 232.3	72 232.4	72 235.6	72 232.6	72 234.8
20	72 262.5	72 262.5	72 262.6		72 262.8	72 264.5
21	72 288.4	72 288.5	72 288.6	72 290.9	72 288.7	72 290.3
22	72 310.9	72 311.0	72 311.0		72 311.2	72 312.5
23	72 330.5	72 330.6	72 330.6		72 330.7	
24	72 347.7	72 347.7	72 347.8		72 347.9	
25	72 362.8	72 362.9	72 362.9		72 363.0	
30	72 417.2	72 417.2	72 417.3		72 417.3	
35	72 449.9	72 449.9	72 450.0		72 450.0	
40	72 471.1	72 471.1	72 471.1		72 471.1	
45	72 485.6	72 485.6	72 485.6		72 485.6	
50	72 496.0	72 496.0	72 496.0		72 496.0	

to the odd 5snp ^{3}P$_{1,2}$ levels (for these n values the $^3P^o_0$ term has merged into the $^3P^o_1$ one). The energies of the following weak line fits well with the value of the 5s$(n-1)$d ^{3}D state: it is a 6s $\rightarrow$ nd forbidden transition and is observed due to the same reasons presented in section 5.1 for explaining their appearance. They emerge here from the background because the second laser is focused. The second weak peak is assigned to the 5snp $^1P^o_1$ state. To summarize, we induce a three-step excitation scheme ($\omega_1+\text{ASE}+\omega_2$) using only two lasers, where the ASE portion of the second laser is responsible for the second resonant transition.

The 5snf $^{1,3}F^o_J$ states were also calculated by the above-described method (section 4). The coincidence of the obtained results with the experimental ones is satisfactory, see table 4. However, in contrast with the experiment, the calculation shows that the singlet terms $^1F^o_3$ are located above the triplet terms $^3F^o_J$. These differences are probably due to the interaction with states with an excited core (for details see section 5.4). The two triplet series ^{3}F$_{2,3}$ merge at $n > 15$ and the ^{3}F$_4$ series associate with them at $n > 19$. At $n > 23$ the triplet and the singlet series merge into each other. For all the calculated states ($n = 4$–50), the quantum defect δ is ~ 0.1. The mixing of both $^{1,3}F^o_3$, $J = 3$ states, for $n = 4$–9, is 55% : 45%. The quantum defects are almost constant in this approximation, with the one corresponding to the singlet series being slightly smaller.

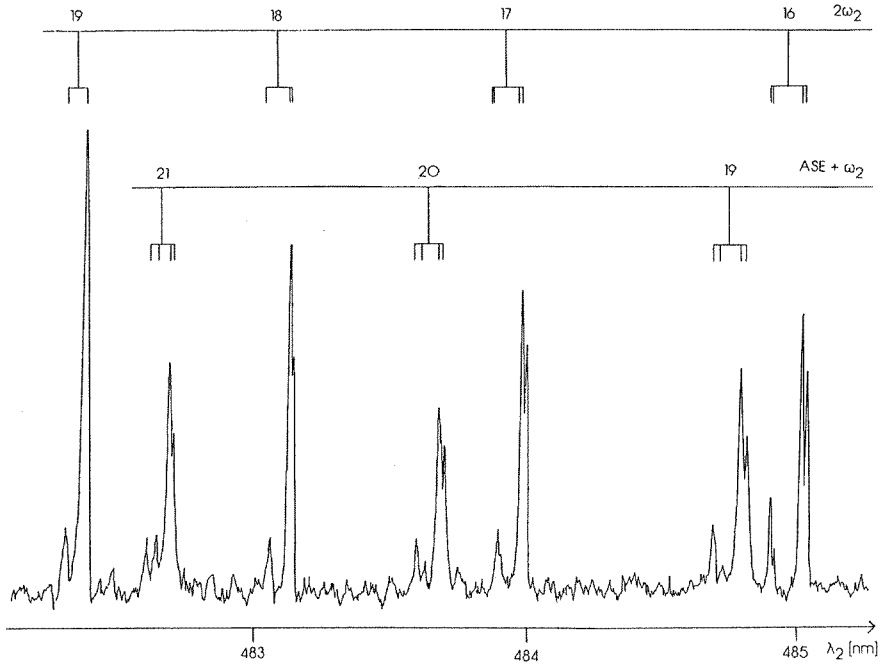

Figure 7. Two-step laser excitation of the 5snp series for medium n values. The $2\omega_2$ spectrum (scheme (c)) overlaps with the ASE $+\ \omega_2$ spectrum.

5.3. Coupling of the valence electrons

For a heavy element the departure from LS coupling with increasing n is essential. A test of this has been performed by Baig (1983) for the Hg atom. We use the same approach. All the investigated terms $e(5sn\mathrm{p}\,^{1,3}\mathrm{P}^{\mathrm{o}}_{J})$ can be expressed as a function of the coupling parameter Φ according to Edlen (1964):

$$\Phi = \frac{^3\mathrm{P}_2 - {}^3\mathrm{P}_0}{^1\mathrm{P}_1 + {}^3\mathrm{P}_1 - 2\,{}^3\mathrm{P}_0}. \tag{8}$$

Figure 8 presents the investigated terms as a function of Φ. For $n < 19$, the calculation (figure 8(a)) demonstrates LS coupling of the states. The extrapolated values are presented in figure 8(b). Note that Φ becomes negative if $^3\mathrm{P}_0 >^3 \mathrm{P}_1 >^3 \mathrm{P}_2$. The absolute value of Φ depends on the mutual location of the terms. Obviously, even for $n = 50$ the coupling scheme of the valence 5s and np electron is rather an LS-coupling than jj-coupling scheme.

5.4. The dipole polarizability of the Cd^+ ion

In what follows, we will give an estimated value for the effective dipole polarizability of the Cd^+ ion from the energy level positions of the 5snf states of the neutral atom. First, one would expect that the nf electron does not penetrate the core, since the highest angular momentum in the Cd^+ core is two. From the lack of other effects, the measured quantum defect would be attributed to the polarization of the ionic core, but our results show the following.

(a) The experimental energies indicate that the singlet 5snf levels lie systematically below the triplet ones. The calculated ones show the opposite effect (see table 4) and agrees

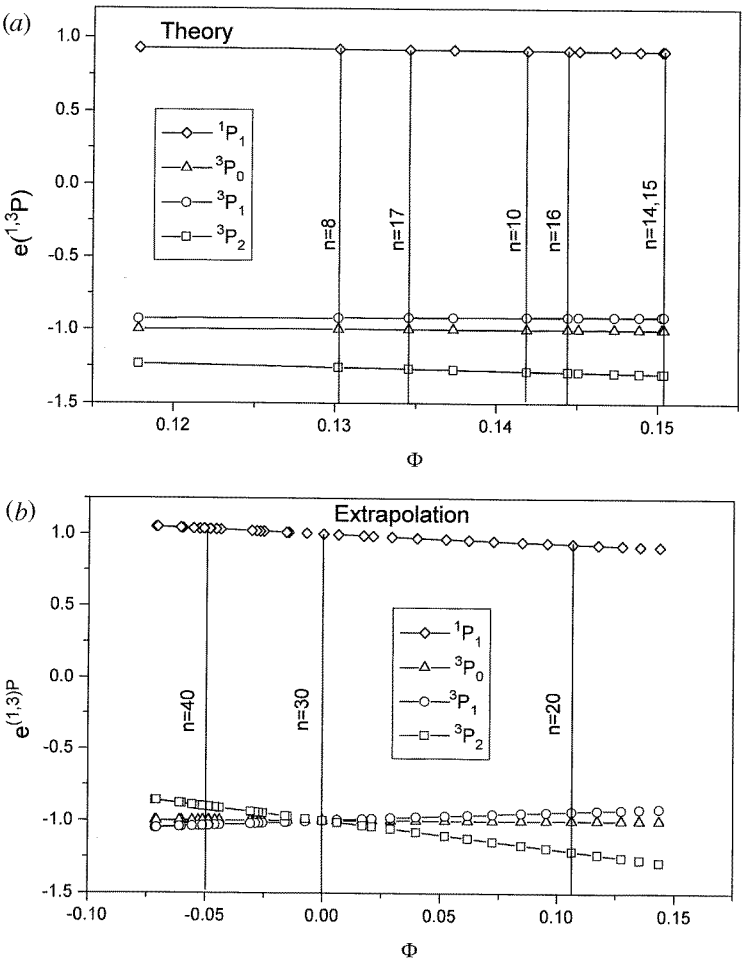

Figure 8. Term energies of the 5s*n*p series as a function of the Edlen parameter Φ, equation (8). (*a*) low and medium *n* values, (*b*) high *n* values.

with what is generally expected (Edlen 1964). We have, therefore, to assume that a perturber that lies above the observed series members, or even above the whole series, is responsible for the depression of the singlet levels. Such a level could be the autoionizing configuration $4d^9 5s^2 5p$ located at 100 000 cm^{-1} (Cowan and Wilson 1991) which may interact stronger with the singlet than with the triplet series. As mentioned in the introduction, this is similar to what has been found for the Cd 5s*n*d states.

(b) In figure 9 the experimental quantum defects (QD) are plotted against *n*. For the singlet series, we observe that the QD is constant in the energy range studied. In contrast, the QD of the triplet series is decreasing for higher *n*, indicating a decreasing contribution of penetration for higher levels. This means that only the 5s*n*f levels with $n > 18$ should be taken into acount for a reliable value of the polarizability. Under the present experimental condition, it was not possible to observe the triplet 5s*n*f series for higher *n* values, since these resonances were blended by the much stronger 5s*n*p peaks, populated by the same excitation scheme.

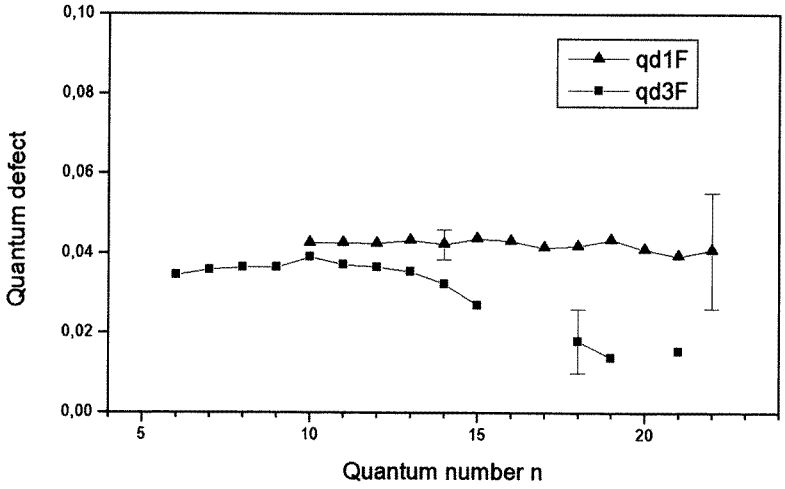

Figure 9. Experimental quantum defects of the 5snf ^{1,3}F^{o} series as a function of n.

To estimate the polarizability α, we consider that the unexcited (inner) 5s electron is the more easily polarized by the outer nf one (Van Vleck and Whitelaw 1933). To calculate the term energy $W(5sn\mathrm{f})$, the two electrons are considered as independent in the zeroth order. In the next approximation (perturbation theory of first order), the dipole term instead of the interelectronic interaction e^2/r_{ij} is used, thus neglecting quadrupole and higher-order polarizabilities. This leads to a simple expression for W,

$$W = W_0 - \tfrac{1}{2}\alpha e^2 \langle n_0 \ell_0 | r^{-4} | n_0 l_0 \rangle \tag{9}$$

where

$$\alpha = -2 \sum_n \frac{|\langle 5\mathrm{s}|r|n\mathrm{p}\rangle|^2}{3W(5\mathrm{s} \rightarrow n\mathrm{p})}$$

is the dipole polarizability. W_0 is the hydrogenic term energy $-RZ^2/n^2$ for non-penetrating orbits, the value $\langle r^{-4} \rangle$ is the hydrogenic value (Bethe and Salpeter 1957) for $\ell_0 = 3$ and $W(5\mathrm{s} \rightarrow n\mathrm{p})$ is the transition energy of the inner 5s electron to the np principal series members.

A number of approximations made, leading to (9), can be justified for Cd:

(1) the core should be an $\ell = 0$ state, which is obvious;

(2) the singlet–triplet 5snf splitting is negligible. Following the discussion (a) and (b) above, we restrict ourselves to a few observed triplet states with $n > 17$. From the calculated 5snf series in table 4 (we notice that no interaction with an autoionizing state was considered in the calculation), we see that for $n > 17$ this splitting becomes of the order of the experimental accuracy. So we can approximate the energy of the triplet 5snf level with the centre of gravity of the 5snf configuration with negligible splitting.

(3) The total energy $W(5sn\mathrm{f} \rightarrow n\mathrm{p}m\ell)$ with $\ell = \mathrm{d}, \mathrm{g}$ is approximated in the calculation by the core electron transition $W(5\mathrm{s} \rightarrow n'\mathrm{p})$. Thus, the above replacement means that the core electron transition is much larger than the transition of the outer nf electron to near-lying nd and ng levels. Inspection of tables 3 and 4 shows that the nf to nd transitions are of the order of 100 cm^{-1} while those to the (unknown) ng ones should be even smaller. On the other hand, the lowest core transition is 44 136.1 cm^{-1} (Moore 1955). We therefore conclude that this condition is also fulfilled for Cd.

If we apply equation (9) for the triplet levels $n = 17$, 18 and 21 with the experimental energies from table 4, the average value for the polarizability is $\alpha = 19\ a_0^3$ in units of the Bohr radius.

Another approach for the polarizability can be obtained from the following formula (Sobelman 1979),

$$\alpha = (e^2/m) \sum (f_{ij}/\omega_{ij}^2) \tag{10}$$

where f_{ij} is the transition oscillator strength of the Cd^+ 5s electron (level i) to the members j of the n'p principal series. e and m are the electron charge and mass, respectively, and $\omega_{ij} = W(5s \rightarrow n'p)$ is the term energy. Thus each term n'p contributes to the polarizability by an amount f_{ij}/ω_{ij}^2. The contributions of the first few terms should provide a good estimation of α, due to both the increasing transition frequencies ω_{ij} and to the rapidly decreasing values of f_{ij} with increasing n' in the n'p Rydberg series. However, it has been shown (Theodosiou 1994) that for the Cd^+ ion there exist almost complete cancellations for all transitions $5s \rightarrow n'p$ except for $n' = 5$ (the resonance transition). Therefore, we can obtain from (10) an accurate enough value for α if we use the data of the two Cd^+ $5p\,^2P_{1/2,3/2}$ levels at 44 136.1 and 46 618.55 cm^{-1}, respectively (Moore 1955). The values for f_{ij} can by obtained from their lifetimes, 3.11 and 2.77 ns, which have been measured recently (Pinnington *et al* 1994). The calculated value for α is then 17.1 a_0^3 in units of the Bohr radius.

Despite the various approximations made to obtain the experimental value of α and the few levels (only three) taken into account, the value of α from our experiment is in good agreement with the one from lifetime measurements. Our value is slightly larger and it may be due to some residual core penetration of the triplet series which contributes in the QD. We have, therefore, to record the triplet 5s*n*f series for higher values of n, but the above discussion shows the limit of our experimental set-up: in order for the nf series to be observed for $n > 25$ the strong np resonances should be suppressed. This may be achieved by applying the same excitation scheme with both laser beams circularly (e.g. σ^+) polarized: the final states would have $J = 3$ and the 5s*n*p levels could not be excited. This would require a collision-free environment, where the polarization of the intermediate state is not destroyed as it is now for the case of our Cd cell. Experiments using a Cd atomic beam are now planned in our laboratory.

6. Conclusion

We have observed the 5s*n*p $^3P_J^o$ Rydberg spectra of cadmium. New data are presented for the $^3P_0^o$ ($n = 9$–19) and $^3P_2^o$ ($n = 11$–50) series, which are resolved for the first time. We have further recorded the 5s*n*f $^{1,3}F_J^o$ Rydberg series for $n = 10$–22 and $n = 4$–21, respectively. Under particular conditions in our experiment, some optically forbidden transitions to series members with the configurations 5s*n*s ^{3}S and 5s*n*d ^{3}D have been recorded, and these have been attributed to an ℓ-mixing mechanism due to a DC Stark effect. The calculations were performed using a perturbation theory with a zero-order model approximation, where the interaction of the two valence electrons has been calculated exactly. This revealed good agreement (deviation 1–2 cm^{-1} for $n = 50$) with the energies of the 5s*n*p states, and satisfactory agreement with the energies of the 5s*n*f state. From the energy level positions of the triplet 5s*n*f states ($n > 18$) we find an approximate value of the effective dipole polarizability of the Cd^+ ion of 19 a_0^3, which, despite many approximations, agrees well with the value calculated from lifetime measurements.

Acknowledgment

We thank Dr C E Theodosiou of the University of Toledo, Ohio, for making his results on the Cd^+ oscillator strengths available to us.

References

Baig M A 1983 *J. Phys. B: At. Mol. Phys.* **16** 1511
Baig M A, Akram M, Bhatti S A, Sommer K and Hormes J 1994 *J. Phys. B: At. Mol. Opt. Phys.* **27** 1693
Bethe H A and Salpeter E E 1957 *Quantum Mechanics of One- and Two-Electron Atoms* (Berlin: Springer) ch 1, p 17
Brown C M, Tilford S G and Ginter M L 1975 *J. Opt. Soc. Am.* **65** 1404
Burkhardt C E, Ciocca M, Garver W P and Leventhal J J 1986 *Phys. Rev. Lett.* **57** 1562
Chantepie M, Cojan L J and Landais J 1975 *J. Physique* **36** 1067
Chantepie M, Cojan L J, Landais J, Laniepce B, Moudden A and Aymar M 1983 *Opt. Comm.* **46** 93
Cowan R D and Wilson M 1991 *J. Phys. B: At. Mol. Opt. Phys.* **24** 111
Edlen B 1964 *Atomic Spectra (Handbuch der Physik 28)* ed S Flugge (Berlin: Springer) pp 80–220
Hashizume A and Wasada N 1980 *J. Phys. B: At. Mol. Phys.* **13** 4865
Jimenez-Mier J, Caldwell C D and Krause M O 1989 *Phys. Rev.* A **39** 95
Kerkhoff H, Schmidt M, Teppner U and Zimmermann P 1980 *J. Phys. B: At. Mol. Phys.* **13** 3969
Kompitsas M, Baharis C and Pan Z 1994 *J. Opt. Soc. Am.* B **11** 697
Laniepce B 1970 *J. Physique* **31** 439
Laniepce B, Landais J and Chantepie M 1976 *Opt. Comm.* **19** 92
Lewis E L 1977 *Am. J. Phys.* **45** 38
Mansfield M W D 1978 *Proc. R. Soc.* A **362** 129
Marr G V and Austin J M 1969 *Proc. R. Soc.* A **310** 137
Martin N L S and Ross K J 1984 *J. Phys. B: At. Mol. Phys.* **17** 4033
Melikechi N and Allen L 1986 *J. Opt. Soc. Am.* B **3** 41
Moore C E 1955 *Atomic Energy Levels (Natl. Standards Ref. Data Ser. Natl. Bur. Standards)* (Washington, DC: US Govt Printing Office) pp 55–8
Pejcev V, Ross K J, Rassi D and Ottley T W 1977 *J. Phys. B: At. Mol. Phys.* **10** 459
Pinnington E H, van Hunen J J, Gosselin R N, Guo B and Berends R W 1994 *Phys. Scr.* **49** 331
Popescu I I, Ghita C, Popescu A and Musa G 1966 *Ann. Phys., Lpz.* **18** 103
Sobelman I I 1979 *Atomic Spectra and Radiative Transitions* (Berlin: Springer) ch 9, p 209
Theodosiou C E 1994 private communication
Van Vleck J H and Whitelaw N G 1933 *Phys. Rev.* **44** 551
Vidolova-Angelova E 1994 *Z. Phys.* D **32** 13
Vidolova-Angelova E 1992 *J. Phys. B: At. Mol. Opt. Phys.* **25** 3735
Vidolova-Angelova E and Ivanov L N 1991 *J. Phys. B: At. Mol. Opt. Phys.* **24** 4147
Wu D H, Yang Y F and Lu K T 1990 *J. Phys. B: At. Mol. Opt. Phys.* **23** L149
Zhang J, Lambropoulos P, Zei D, Compton R N and Stockdale J A D 1992 *Z. Phys.* D **23** 219
Zhang J Y and Lu K T 1987 *J. Phys. B: At. Mol. Phys.* **20** 5065